SURFACE CHEMISTRY

Designing durable icephobic surfaces

Kevin Golovin,[1,2] Sai P. R. Kobaku,[2,3] Duck Hyun Lee,[1,2] Edward T. DiLoreto,[1,2] Joseph M. Mabry,[4] Anish Tuteja[1,2,3,5]*

10.1126/sciadv.1501496

Ice accretion has a negative impact on critical infrastructure, as well as a range of commercial and residential activities. Icephobic surfaces are defined by an ice adhesion strength τ_{ice} < 100 kPa. However, the passive removal of ice requires much lower values of τ_{ice}, such as on airplane wings or power lines (τ_{ice} < 20 kPa). Such low τ_{ice} values are scarcely reported, and robust coatings that maintain these low values have not been reported previously. We show that, irrespective of material chemistry, by tailoring the cross-link density of different elastomeric coatings and by enabling interfacial slippage, it is possible to systematically design coatings with extremely low ice adhesion (τ_{ice} < 0.2 kPa). These newfound mechanisms allow for the rational design of icephobic coatings with virtually any desired ice adhesion strength. By using these mechanisms, we fabricate extremely durable coatings that maintain τ_{ice} < 10 kPa after severe mechanical abrasion, acid/base exposure, 100 icing/deicing cycles, thermal cycling, accelerated corrosion, and exposure to Michigan wintery conditions over several months.

INTRODUCTION

Ice accretion and its subsequent removal is a safety hazard for aircrafts, power lines, motor vehicles, marine structures, communication towers, and wind turbines (*1*). The most common methods for ice removal are extremely energy-intensive (*2*), and there exists a strong need to develop methods where ice is passively removed from a surface (that is, no external energy input) (*3*).

Previously, there have been numerous publications related to developing "icephobic" surfaces (*2*–*13*). Such surfaces use different approaches including delaying droplet freezing time (*5*, *13*–*15*), preventing frost formation (*6*, *8*, *12*), and lowering τ_{ice} (*2*–*4*, *6*–*9*, *11*, *13*, *16*). Icephobic surfaces can be defined by an ice adhesion strength τ_{ice} < 100 kPa (*13*). In comparison, structural materials like aluminum or steel have extremely high τ_{ice}, around 1600 and 1400 kPa, respectively (*3*). However, to passively remove ice with no external energy input, such as on airplane wings, power lines, or boat hulls, extremely low values of τ_{ice} are required. For example, Dou *et al.* (*16*) found that a strong breeze detached ice when $\tau_{ice} \leq 27 \pm 6$ kPa.

Previous work has shown that, on different, high modulus solids, $\tau_{ice} = B\gamma(1 + \cos\theta_{rec})$, where B is an experimental constant, γ is the surface tension of water, and θ_{rec} is the receding water contact angle (*2*). For nontextured surfaces, this provides a theoretical lower limit for τ_{ice} of ~150 kPa (as the maximum $\theta_{rec}^{water} \approx 120°$). Superhydrophobic surfaces display an ultrahigh θ_{rec}^{water} through the incorporation of texture and have been shown to have τ_{ice} as low as 50 kPa. However, an increasing body of work suggests that even these moderately low ice adhesion values cannot be maintained due to condensation and frost formation (*5*, *6*, *13*–*15*, *17*). To date, the lowest ice adhesion values have only been reported using lubricants (τ_{ice} = 16 kPa) or gels (τ_{ice} = 0.4 kPa) (*8*, *18*–*20*). Lubricated surfaces purportedly achieve low ice adhesion by minimizing the contact angle hysteresis on the surface through the formation of a low surface energy (typically highly fluorinated) lubricating free-oil layer. But again, the icephobicity for such surfaces can be short-lived, as the oil may be displaced and removed by water droplets (*7*) or frost (*12*), or during accreted ice removal (fig. S1A). Overall, there are no reports of durable icephobic surfaces that maintain or even exhibit τ_{ice} < 15 kPa.

Here, we study the ice adhesion of elastomers. Elastomers are viscoelastic, that is, they can demonstrate both solid- and liquid-like properties. We control the viscoelastic nature of our elastomers in two ways. First, we modify the cross-link density ρ^{CL} of our elastomers to alter their physical stiffness ($G = RT\rho^{CL}$, assuming isotropy, where G is the shear modulus and R is the universal gas constant). The stress required to shear a hard block (such as ice) from a soft film (such as an elastomeric coating) is given by $\tau = A(W_a G/t)^{1/2}$, where A is an experimental constant, W_a is the work of adhesion, and t is the thickness of the soft film (*21*, *22*). This is a macroscopic relationship that predicts the shear stress required to cleave two surfaces apart, a process that occurs through interfacial cavitation (*21*, *23*).

Second, we alter the no-slip boundary condition (*24*) at the ice-elastomer interface through the addition of uncross-linked, polymeric chains. In solid-solid contact, conservation of momentum usually dictates that the velocity at the interface is zero or that there is no slip. However, if the polymeric chains within the elastomer are sufficiently mobile, slippage (that is, a nonzero slip velocity) can occur at the solid-solid interface, as has been observed previously for polymer melts (*25*, *26*), adhesives (*24*), and rubbers (*23*). When a hard surface slides over a soft elastomer, such as during interfacial slippage, the shear stress to slip at the interface is given by $\tau = Gfa/kT$ or $\tau \propto G^1$. Here, f is the force needed to detach a single chain of segmental length a, k is the Boltzmann's constant, and T is the temperature (*27*, *28*). By tailoring ρ^{CL} for different elastomeric coatings, and by additionally embedding miscible, polymeric chains to enable interfacial slippage, we show that it is possible to systematically design icephobic coatings with extremely low ice adhesion (τ_{ice} < 0.2 kPa). Overall, we have designed a comprehensive library of more than 100 icephobic surfaces that can be rough, smooth, hydrophobic, or hydrophilic, as shown in fig. S2A (also see Table 1). It is clear from fig. S2 that the variations in τ_{ice} for the different icephobic coatings developed in this work cannot

[1]Department of Materials Science and Engineering, University of Michigan, Ann Arbor, MI 48109, USA. [2]Biointerfaces Institute, University of Michigan, Ann Arbor, MI 48109, USA. [3]Department of Macromolecular Science and Engineering, University of Michigan, Ann Arbor, MI 48109, USA. [4]Rocket Propulsion Division, Air Force Research Laboratory, Edwards Air Force Base, CA 93524, USA. [5]Department of Chemical Engineering, University of Michigan, Ann Arbor, MI 48109, USA.
*Corresponding author. E-mail: atuteja@umich.edu

Table 1. A library of icephobic surfaces. The coating fabrication methodology and resulting ice adhesion strengths, cross-link densities, and water contact angles for all the samples fabricated in this work. SG, Sylgard; SO, silicone oil; PS, polystyrene; PIB, polyisobutylene; PFPE, perfluoropolyethers; FPU, fluorinated polyurethane polyols; PMPS, polymethylphenyl siloxane; UVA, ultraviolet A; RT, room temperature; NS, no slippage (no oil is added to the coating); IS, interfacial slippage (miscible oil has been added but no lubricating liquid layer forms) [confirmed by atomic force microscopy (AFM), optical microscopy, and the shape of the force versus time curves]; L, lubricated [excess oil (either intentionally or otherwise) is added to the coating, forming a thick lubricating layer] (confirmed using the same methods as for interfacial slippage).

	Polymer base	Nonreactive oil	wt %	Reactive oil	wt %	Cure (°C/hour)	ρ^{CL} (mol/m^3)	τ_{ice} average (kPa)	τ_{ice} min. (kPa)	τ_{ice} max. (kPa)	Type	$\theta_{adv}/\theta_{rec}$ (°)
A	SG 184 10:1	—	—	—	—	150/24	307±8	264	245	340	NS	120/94
B	SG 184 10:1	—	—	—	—	80/2	333±45	47	36	57	IS	131/26
C	SG 184 20:1	—	—	—	—	80/2	112±1	178	147	251	NS	129/45
D	SG 184 4:1	—	—	—	—	80/2	33±45	89	42	165	IS	127/36
E	SG 184 3:1	—	—	—	—	80/2	268±2	15	6	29	L	122/76
F	SG 184 2:1	—	—	—	—	80/2	222±9	14	6	23	L	118/77
G	SG 184 5:2	—	—	—	—	80/2	267±21	16	8	26	L	112/100
H	SG 184 1:1	—	—	—	—	80/2	162±5	14	6	29	L	112/89
I	SG 184 10:1	100-cP SO	25	—	—	80/2	219±13	35	26	56	IS	123/89
J	SG 184 10:1	100-cP SO	50	—	—	80/2	72±11	87	40	120	IS	114/94
K	SG 184 10:1	100-cP SO	75	—	—	80/2	—	55	30	71	IS	114/94
L	SG 184 10:1	—	—	PMHS	25	80/2	215±10	10	1.0	31	L	105/103
M	SG 184 10:1	—	—	PMHS	50	80/2	75±13	67	31	121	IS	118/101
N	SG 184 10:1	—	—	PMHS	75	80/2	—	17	4.9	39	L	121/102
O	SG 184 1:1	100-cP SO	25	—	—	80/2	32±2	173	58	237	IS	124/86
P	SG 184 1:1	100-cP SO	50	—	—	80/2	13±2	46	17	74	IS	124/82
Q	SG 184 1:1	100-cP SO	75	—	—	80/2	—	18	0.15	47	IS	104/103
R	SG 184 1:1	—	—	PMHS	25	80/2	102±5	17	1.0	40	L	125/104
S	SG 184 1:1	—	—	PMHS	50	80/2	14±4	6	0.7	30	L	106/105
T	SG 184 1:1	—	—	PMHS	75	80/2	—	9	0.35	31	L	105/103
U	SG 184 10:1	100-cP SO	25	PMHS	25	150/24	536±97	64	50	78	IS	119/95
V	SG 184 10:1	100-cP SO	15	PMHS	15	80/2	—	31	1.0	137	L	108/104
W	SG 184 10:1	100-cP SO	10	PMHS	10	150/24	459±9	74	40	116	IS	123/90
X	SG 184 10:1	—	—	PMHS	10	80/2	283±9	37	4.0	71	IS	114/100
Y	SG 184 10:1	—	—	PMHS	10	150/24	284±41	173	122	234	NS	121/78
Z	SG 184 10:1	—	—	PMHS	20	80/2	197±4	45	19	82	IS	109/105
AA	SG 184 10:1	—	—	PMHS	20	150/24	348±28	64	34	92	IS	118/93
BB	SG 184 10:1	—	—	PMHS	25	150/24	452±9	302	275	346	NS	103/84
CC	SG 184 10:1	100-cP SO	25	PMHS	15	150/24	405±27	58	41	73	IS	112/104
DD	SG 184 10:1	100-cP SO	20	PMHS	20	80/2	107±2	37	9.1	67	IS	109/100
EE	SG 184 10:1	100-cP SO	25	PMHS	25	80/2	150±8	35	5.1	77	IS	116/99
FF	SG 184 10:1	100-cP SO	25	PMHS	10	150/24	290±25	41	24	55	IS	112/108
GG	SG 184 10:1	5-cP SO	25	—	—	80/2	181±5	145	109	178	IS	121/90

continued on next page

	Polymer base	Nonreactive oil	wt %	Reactive oil	wt %	Cure (°C/hour)	ρ^{CL} (mol/m^3)	τ_{ice} average (kPa)	τ_{ice} min. (kPa)	τ_{ice} max. (kPa)	Type	$\theta_{adv}/\theta_{rec}$ (°)
HH	SG 184 10:1	1000-cP SO	25	—	—	80/2	153±7	45	33	53	IS	100/85
II	SG 184 10:1	10000-cP SO	25	—	—	80/2	67±2	81	13	226	L	120/104
JJ	SG 184 10:1	SO AP 1000	25	—	—	80/2	216±3	66	12	171	L	113/78
KK	SG 527 1:1	—	—	—	—	150/24	0.68‡	14	7.6	25	NS	130/89
LL	1:9 SG 527:184	100-cP SO	25	—	—	150/24	182±11	14	7.3	18	IS	112/103
MM	1:3 SG 527:184	100-cP SO	25	—	—	150/24	123±2	10	5.5	17	IS	111/104
NN	1:1 SG 527:184	100-cP SO	25	—	—	150/24	76±1	9	5.5	12	IS	112/102
OO	3:1 SG 527:184	100-cP SO	25	—	—	150/24	46±2	6	3.7	8	IS	114/101
PP	3:1 SG 527:184	—	—	—	—	150/24	50±2	10	4	49	IS	123/100
QQ	1:3 SG 527:184	—	—	—	—	150/24	104±5	141	130	154	NS	122/95
RR	1:1 SG 527:184	—	—	—	—	150/24	110±5	19	6.7	37	IS	117/88
SS	9:1 SG 527:184	100-cP SO	25	—	—	150/24	8.0±0.8	6	4.1	7	IS	121/98
TT	9:1 SG 527:184	—	—	—	—	150/24	9.1±0.9	134	132	139	NS	121/96
UU	PFPE	—	—	—	—	UVA 5 min	160±35	238	200	281	NS	115/93
VV	PFPE	Krytox 100	25	—	—	UVA 5 min	96±24	31	17	53	IS	115/95
WW	PFPE	Krytox 105	25	—	—	UVA 5 min	124±33	31	16	55	IS	104/98
XX	PFPE	Krytox 103	25	—	—	UVA 5 min	—	12	10	13	IS	114/91
YY	PFPE	—	—	CN4002	10	UVA 5 min	—	45	33	51	L	117/91
ZZ	FPU	—	—	—	—	80/72	1098±98	538	257	627	NS	103/72
AB*	FPU	—	—	—	—	80/72	475±14	394	334	479	NS	105/73
AC*	FPU	—	—	—	—	80/72	316±17	284	204	399	NS	101/73
AD*	FPU	Krytox 100	25	—	—	80/72	1142±158	595	538	713	IS	101/72
AE*	FPU	Krytox 105	25	—	—	80/72	1112±77	392	283	520	IS	105/72
AF*	FPU	—	—	NCO C50	75	150/24	1332±48	246	194	320	IS	108/84
AG*	FPU	100-cP SO	5	NCO C50	75	80/72		82	61	100	IS	109/82
AH*	FPU	100-cP SO	10	NCO C50	75	80/72		49	22	66	IS	106/96
AI	PS	—	—	—	—	RT/24	447,000‡	336	189	370	NS	97/86
AJ	PS	200 M_w PS	25	—	—	RT/24	—	424	271	569	IS	103/74
AK	PS	200 M_w PS	50	—	—	RT/24	—	570	378	642	IS	109/58
AL	PS	540 M_w PS	25	—	—	RT/24	—	477	454	510	IS	100/79
AM	PS	SO AP 1000	25	—	—	RT/24	—	92	59	112	L	103/97
AN	PS	PMPS	10	—	—	RT/24	—	354	218	491	IS	98/84
AO	PS	PMPS	5	—	—	RT/24	—	333	217	498	IS	99/84
AP	PIB	—	—	—	—	RT/24	8,000‡	395	335	453	NS	125/56
AQ	PIB	Polybutene	25	—	—	RT/24	—	288	220	419	IS	128/56
AR	PIB	Polybutene	50	—	—	RT/24	—	459	341	620	IS	130/17
AT	PIB	Polybutene	75	—	—	RT/24	—	268	176	442	IS	128/72
AU	VytaFlex10	—	—	—	—	RT/24	26±7	144	84	254	NS	52/12

continued on next page

	Polymer base	Nonreactive oil	wt %	Reactive oil	wt %	Cure (°C/hour)	ρ^{CL} (mol/m^3)	τ_{ice} average (kPa)	τ_{ice} min. (kPa)	τ_{ice} max. (kPa)	Type	$\theta_{adv}/\theta_{rec}$ (°)
AV	VytaFlex40	—	—	—	—	RT/24	95±14	151	118	192	NS	80/26
AW	VytaFlex60	—	—	—	—	RT/24	290±17	261	157	360	NS	82/23
AX†	VytaFlex40	Vegetable	20	—	—	RT/24	53±4	10.5	4.6	22	L	68/21
AY*	VytaFlex40	Cod liver	15	—	—	RT/24	29±2	27	9	51	IS	75/12
AZ*	VytaFlex40	100-cP SO	10			RT/24	—	41	18	83	L	82/45
BA	VytaFlex40	—	—	NCO Di-50	1	RT/24	47±3	109	51	179	IS	96/49
BB	VytaFlex40	—	—	NCO Di-50	5	RT/24	52±2	101	42	232	IS	110/56
BC	VytaFlex40	—	—	NCO Di-50	10	RT/24	34±7	139	49	243	IS	113/60
BD*	VytaFlex40	100-cP SO	10	NCO Di-100	50	RT/24	21±1	11	6	15	IS	97/89
BE*	VytaFlex40	—	—	NCO C50	50	RT/24	42±0.4	44	25	55	IS	106/81
BE†	VytaFlex40	100-cP SO	5	NCO C50	50	RT/24		36	18	57	IS	100/85
BF*	VytaFlex40	100-cP SO	10	NCO C50	50	80/72		11	6	17	IS	95/86
BG*	VytaFlex40	—	—	NCO C50	75	RT/24	171±4	49	38	65	IS	102/85
BH*	VytaFlex40	100-cP SO	10	NCO C50	75	RT/24		9	3	12	IS	91/82
BI*	VytaFlex40	1000-cP SO	10	NCO C50	75	RT/24		10	5	14	IS	99/90
BJ*	VytaFlex40	5-cP SO	10	NCO C50	75	RT/24		18	12	24	IS	102/83
BK	VytaFlex40	10,000-cP SO	10	NCO C50	75	RT/24		19	14	31	IS	102/92
BL	VytaFlex40	100-cP SO	5	—	—	RT/24	—	77	70	90	L	70/42
BM	VytaFlex40	100-cP SO	10	—	—	RT/24	—	80	58	91	L	68/42
BN	VytaFlex40	100-cP SO	15	—	—	RT/24	—	98	68	128	L	65/41
BO	VytaFlex40	100-cP SO	20	—	—	RT/24	—	93	76	107	L	67/42
BO	VytaFlex40	Vegetable	5	—	—	RT/24	62±2	128	77	200	IS	79/23
BQ	VytaFlex40	Vegetable	10	—	—	RT/24	62±4	238	233	247	IS	89/48
BR	VytaFlex40	Vegetable	15	—	—	RT/24	49±2	121	91	151	IS	32/20
BS	VytaFlex40	Vegetable	20	—	—	RT/24	53±4	173	141	227	IS	43/34
BT	VytaFlex40	Cod liver	5	—	—	RT/24	—	129	107	166	IS	67/29
BU	VytaFlex40	Cod liver	10	—	—	RT/24	—	70	56	85	IS	59/34
BV	VytaFlex40	Cod liver	15	—	—	RT/24	—	110	100	120	IS	46/34
BW†	VytaFlex40	Cod liver	15	—	—	RT/24	29±2	4	2	9	IS	43/25
BX†	VytaFlex40	Vegetable	15	—	—	RT/24	52±1	11	3	15	IS	88/44
BY†	VytaFlex40	Safflower	2.5	—	—	RT/24	63±0.5	30	20	43	IS	100/32
BZ*	VytaFlex40	Safflower	5	—	—	RT/24	50±0.5	11	9	16	IS	82/28
BA*	VytaFlex40	Safflower	10	—	—	RT/24	45±5	6	4	12	IS	72/24
CB†	VytaFlex40	Safflower	15	—	—	RT/24	33±1	4	1	7	IS	67/29
CC†	VytaFlex40	Safflower	20	—	—	RT/24	32±0.4	6	3	11	L	56/44
CD†	VytaFlex40	Safflower	25	—	—	RT/24	45±2	4	2	6	L	52/43
CE	VytaFlex40	Cod liver	20	—	—	RT/24	—	97	76	114	L	34/21

*Films that were spray-coated (500 mg/ml). All others are spin-cast at 1500 rpm for 60 s (200 mg/ml). †Films that were dip-coated (500 mg/ml). ‡Approximated from the elastic modulus of the polymer.

be explained by variations in the parameter $1 + \cos\theta_{rec}$. For soft surfaces, this is because the interface either cavitates or slips before the work of adhesion is reached (*21*).

RESULTS AND DISCUSSION

Mechanisms for low ice adhesion

We first attempted to understand the effects of interfacial slippage and ρ^{CL} on τ_{ice}, using a shear-based (Mode-II) ice adhesion test, conducted at −10°C (see Materials and Methods) (*2*). To do so, we tested four representative polydimethylsiloxane (PDMS) samples: high ρ^{CL} PDMS (ρ^{CL} = 307 ± 8 mol/m^3), low ρ^{CL} PDMS (ρ^{CL} = 50 ± 2 mol/m^3), high ρ^{CL} PDMS with oil (ρ^{CL} = 290 ± 25 mol/m^3, 25 wt % silicone oil), and low ρ^{CL} PDMS with oil (ρ^{CL} = 46 ± 2 mol/m^3, 25 wt % silicone oil). For high ρ^{CL} PDMS (unaltered Sylgard 184), τ_{ice} = 264 ± 19 kPa (Fig. 1A), which matches reported literature values of 200 to 300 kPa (*2*, *10*). To achieve a surface with interfacial slippage and the same ρ^{CL} as Sylgard 184, we added both silicone oil (which lowers ρ^{CL}) and polymethylhydrosiloxane (PMHS; which raises ρ^{CL}) until the equivalent ρ^{CL} was achieved. Such a surface has τ_{ice} = 58 ± 5 kPa, a fivefold reduction over unaltered Sylgard 184, highlighting the effect of interfacial slippage provided by the miscible chains. Note that by maximizing the miscibility between the elastomeric network and the chains causing interfacial slippage, we avoid the formation of a liquid layer on top of the substrate that can be easily abraded (discussed later) (*6*, *7*, *12*). For PDMS with a lower ρ^{CL} and devoid of any uncross-linked chains (see Materials and Methods), we found τ_{ice} = 33 ± 2 kPa. This is five times lower than the theoretical minimum of τ_{ice} = 150 kPa, without the use of lubricating layers, fluorination, or texture. Indeed, coatings with values of τ_{ice} < 10 kPa can be fabricated without oil, solely by lowering ρ^{CL} significantly (see coatings KK, PP, and RR in Table 1). Similarly, chemically grafted chains that can induce interfacial slippage can lower the ice adhesion to values as low as τ_{ice} = 11 ± 4 kPa (fig. S1D). Both mechanisms can be used independently to fabricate surfaces with lower ice adhesion than anything previously reported. Indeed, when both mechanisms are used in concert, these effects are amplified. Accordingly, for low ρ^{CL} PDMS with interfacial slippage, we measured τ_{ice} = 6 ± 1 kPa.

We fabricated a series of different icephobic coatings (see Materials and Methods) from PDMS, polyurethane rubbers (PU), fluorinated polyurethane polyols (FPU), and perfluoropolyethers (PFPE), with ρ^{CL} varying from 0.68 to 1203 mol/m^3, as measured by solvent swelling using Flory-Huggins theory (*29*) and confirmed by Mooney-Rivlin analysis (fig. S3) (*30*). To enable interfacial slippage, we embedded the elastomers with either silicone, Krytox, vegetable oil, cod liver oil, or safflower oil (see Materials and Methods). Earlier, we stated that $\tau_{ice} \propto G^{1/2}$ for elastomeric surfaces in the absence of interfacial slippage. When we measured τ_{ice} for surfaces devoid of any uncross-linked chains (that is, no added oil), we observe this dependence precisely (Fig. 1B). Because of interfacial cavitation, the

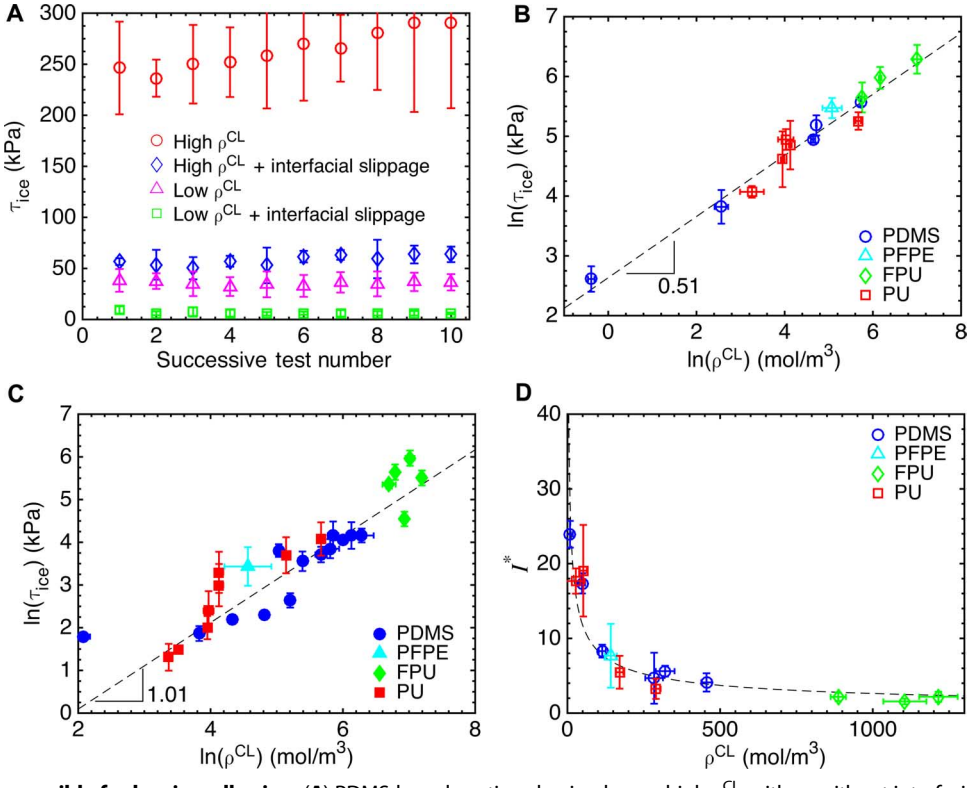

Fig. 1. Mechanisms responsible for low ice adhesion. (**A**) PDMS-based coatings having low or high ρ^{CL}, with or without interfacial slippage. (**B**) Relationship between ρ^{CL} and τ_{ice} for coatings without interfacial slippage. Error bars are 1 SD, and the best fit is found using the method proposed by York *et al.* (*44*). The slope is 0.51 ± 0.04. (**C**) Variation of τ_{ice} with ρ^{CL} for coatings with interfacial slippage. The best-fit slope is 1.01 ± 0.03. (**D**) Ice-reducing potential I^* as a function of ρ^{CL}. Error bars are 1 SD, and for the best-fit curve shown, R^2 = 0.89.

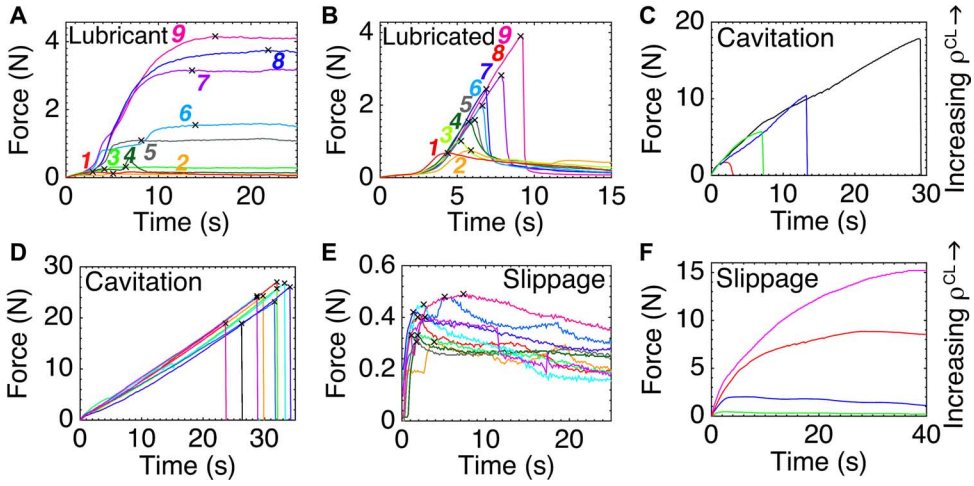

Fig. 2. Force versus time curve analysis. (**A** and **B**) Force versus time curves for a lubricant (PMHS oil) and lubricated (coating R) surfaces. The number next to each curve is the order in which the testing was performed. (**C**) Representative surfaces from fig. S1B, where the ice unadheres by interfacial cavitation. Note the abrupt drop in force once the ice has detached. Depending on the cross-link density, the ice adhesion can be low or high, but the mechanism for detachment remains the same. (**D**) The FPU (coating ZZ), which has no uncross-linked chains, causes ice to detach by interfacial cavitation, which results in high but consistent ice adhesion values. (**E**) In contrast, the PU coating (ρ^{CL} = 33 ± 1 mol/m^3, 15 wt % safflower oil) shows interfacial slippage. Note the persistence of a nonzero sliding force long after the ice has moved from its original location. Comparing (A) to (E), it is apparent that lubricated surfaces lose their oily layer quite rapidly, transitioning to high ice adhesion surfaces. (**F**) In contrast, varying the cross-link density on surfaces exhibiting interfacial slippage, the τ_{ice} values can also be low or high, but the mechanism for detachment remains the same.

ice abruptly detached from these coatings (Fig. 2B). For the different elastomers tested here, we found no significant impact of elastomer chemistry/surface energy on τ_{ice}. The variation in ice adhesion strength was dominated by the changes in ρ^{CL}.

When interfacial slippage is enabled, $\tau_{ice} \propto G^1$, assuming perfect molecular contact between the ice and the coated substrate (*27*). As we started with liquid water that was subsequently frozen, this assumption should hold. We confirmed this linear relationship for a number of different icephobic systems, as shown in Fig. 1C. Because of the interfacial slippage, the frictional force persisted long after the ice had unadhered from its original location (see Fig. 2, E and F). Thus, we can differentiate elastomers with and without interfacial slippage either by the dependence of τ_{ice} on ρ^{CL} or by comparing the shape of their force versus time curves over multiple icing/deicing cycles. To predict the ice adhesion strength–reducing potential of interfacial slippage for different elastomers, we developed the dimensionless parameter I^* (see the Supplementary Materials). I^* is the ratio between τ_{ice} for an elastomer without ($\tau_{ice}^{no\text{-}slip}$) and with interfacial slippage (τ_{ice}^{slip}), and is given as

$$I^* = \frac{\tau_{ice}^{no\text{-}slip}}{\tau_{ice}^{slip}} = \frac{C}{\sqrt{\rho^{CL}}} \quad (1)$$

where C is a constant. For 14 different elastomeric surfaces (see Materials and Methods), we precisely made samples with equivalent ρ^{CL}, both with and without interfacial slippage. Our measured I^* values match the trend predicted by (Eq. 1) quite well (Fig. 1D). The two important points to note here are that (i) a low ρ^{CL} can help achieve extremely low values of τ_{ice} and (ii) interfacial slippage is most effective in lowering τ_{ice} for surfaces having a low ρ^{CL}. For example, enabling interfacial slippage for the FPU (ρ^{CL} = 1098 mol/m^3) only gives I^* = 1.6, whereas for soft PDMS (ρ^{CL} = 8.5 mol/m^3), I^* = 24. Moreover, by fitting the data shown in Fig. 1D, we find that $C \approx 83$ mol$^{1/2}$ m$^{-3/2}$. This has the physical interpretation that, for $\rho^{CL} >$ 7000 mol/m^3, the addition of oil (or enabling interfacial slippage) will have no effect on τ_{ice} (see fig. S2B). The cross-linked network with such a high ρ^{CL} is too stiff to allow for significant chain mobility. I^* predictions from (Eq. 1) work well even for systems that only have physical entanglements. For example, adding 25, 50, or 75 wt % liquid polybutene to polybutadiene (ρ^{CL}, ~8000 mol/m^3) (*31*) resulted in statistically equivalent τ_{ice} values as compared to polybutadiene with no embedded polybutene, that is, I^* = 1.0. The same was found for PS (ρ^{CL}, ~450,000 mol/m^3) (*31*) embedded with liquid, low–molecular weight PS (see Materials and Methods; Table 1).

When designing surfaces with interfacial slippage, a thick, lubricating layer can form if the added oil/polymeric chains start to phase-separate from the elastomer. We performed a number of experiments to differentiate lubricated surfaces from surfaces with interfacial slippage. The easiest way to check for a lubricating layer is touching the surface by hand. The layer can also be detected through controlled abrasion or by repeatedly measuring τ_{ice} over multiple icing/deicing cycles (Fig. 3A). This free liquid layer is also readily viewable in optical micrographs or AFM phase images (Fig. 3, C and D). Lubricated systems are also mechanistically different from surfaces with interfacial slippage because they rely on extremely low contact angle hysteresis (CAH) to achieve their properties (*8*). Further, the friction on lubricated surfaces is independent of ρ^{CL} but heavily reliant on the oil viscosity (*32*). In contrast, our icephobic surfaces using interfacial slippage can have high CAH (Table 1), survive harsh mechanical abrasion that should remove any lubricating surface layer (discussed below), display τ_{ice} values that depend strongly on ρ^{CL} (Fig. 1, B to D), and are independent of oil viscosity (Fig. 3B).

Initially, we stated that superhydrophobic surfaces may not be icephobic due to wetting of their porous texture by condensing water droplets or frost. However, if the icephobicity arises from low ρ^{CL}

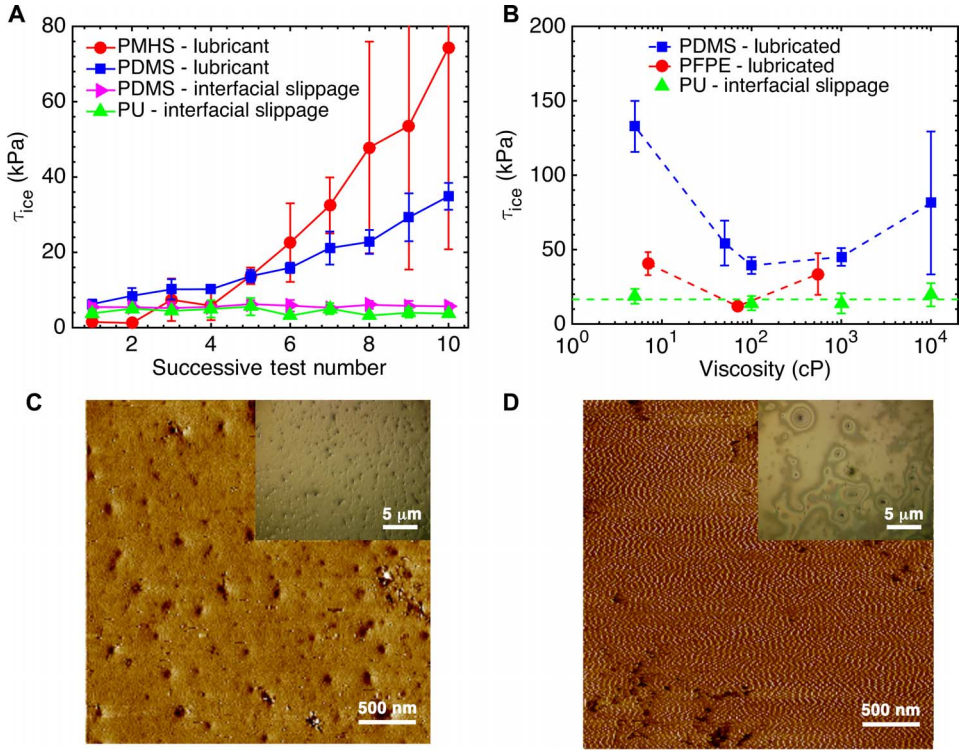

Fig. 3. Comparison between interfacial slippage and lubrication. (**A**) Variation of τ_{ice} with the number of icing/deicing cycles. See Materials and Methods for a description of each coating's fabrication. The values of τ_{ice} for both the lubricant and the lubricated systems increase with an increasing number of icing/deicing cycles (see Fig. 2, A and B, for force versus time curves). In comparison, there is no change in τ_{ice} values for the surfaces with interfacial slippage over multiple icing/deicing cycles. (**B**) Variation in τ_{ice} with oil viscosity. Values of τ_{ice} for lubricated surfaces strongly depend on the oil viscosity and follow a typical Stribeck relationship (*32*). In comparison, the values of τ_{ice} for surfaces with interfacial slippage are markedly independent of viscosity (coatings BH, BI, BJ, and BK in Table 1). (**C**) AFM phase images and optical micrographs of the PU coating with 15 wt % safflower oil. The surface does not have a lubricating oil layer. Note that the AFM phase image looks equivalent to the PU coating without oil (fig. S4C). (**D**) AFM phase images and optical micrographs of the PU coating with 10% silicone oil. The lubricating oil layer is clearly visible on the surface.

and interfacial slippage, superhydrophobic surfaces can be icephobic, even when fully wetted. Using a silicon mold with a square array of holes, we fabricated icephobic (τ_{ice} = 26 ± 3 kPa), PDMS-based micropillars (see Materials and Methods). Droplets of water placed on such a surface display superhydrophobicity, with $\theta^{adv}_{water}/\theta^{rec}_{water}$ = 165°/161° and a low roll-off angle of 3° (Fig. 4). Such surfaces effectively repel water (above 0°C) through minimizing the solid-liquid contact area and solid ice (below 0°C) through low ρ^{CL} and interfacial slippage. The differing mechanisms allow for a superhydrophobic surface to remain icephobic even when the surface is fully frosted. The PDMS-based coatings can also be used to imbue icephobicity to other textured surfaces, such as different wire meshes, yielding values as low as τ^{mesh}_{ice} = 2.4 ± 0.5 kPa (fig. S5).

Durability of icephobic coatings

To initially characterize the durability of our icephobic coatings, we evaluated force versus time curves, and thereby τ_{ice}, for our surfaces over repeated icing/deicing cycles (see Materials and Methods). For surfaces damaged during the icing/deicing process, the shape of the force versus time curves changes, and τ_{ice} increases, with increasing icing/deicing cycles. Both lubricated surfaces, as well as surfaces too soft to prevent physical damage, display such behavior within

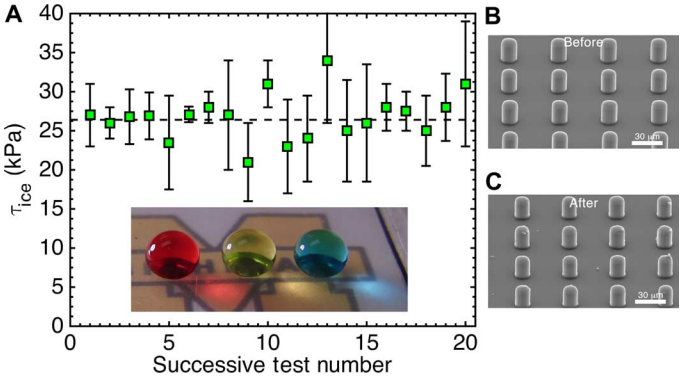

Fig. 4. Superhydrophobic and icephobic surfaces. (**A**) Droplets of water placed on icephobic PDMS pillars (coating I in Table 1) display superhydrophobicity, with $\theta^{adv}_{water}/\theta^{rec}_{water}$ = 165°/161° and a low roll-off angle of 3° (inset). For 20 successive icing/deicing cycles on such surfaces, we measured τ_{ice} = 26 ± 3 kPa. Such surfaces effectively repel liquid water through minimizing the solid-liquid contact area and solid ice through low ρ^{CL} and interfacial slippage. The differing mechanisms allow the surface to remain icephobic even after the surface is fully frosted. (**B** and **C**) SEM micrograph of the icephobic pillars before and after ice adhesion testing. The pillars are not removed during ice adhesion testing.

10 icing/deicing cycles (Figs. 2, A and B, and 3A). However, these soft surfaces often offer almost immeasurably low τ_{ice}. We measured τ_{ice} = 0.15 ± 0.05 kPa for our most icephobic surface (fig. S1B). This is one of the lowest τ_{ice} reported thus far and over five orders of magnitude below τ_{ice} for aluminum. Ice slides off such surfaces solely under its own weight (movie S1). However, additional icing/deicing cycles begin to degrade the surface, raising τ_{ice} (fig. S1B). Durable surfaces with interfacial slippage, typically having higher ρ^{CL}, maintain their low ice adhesion values (τ_{ice} = 3.6 ± 1.0 kPa) over repeated icing/deicing cycles (Fig. 3A) and show self-similar force versus time curves (Fig. 2E).

To illustrate the significant advantage of coatings that repel ice through low ρ^{CL} in conjunction with interfacial slippage, we conducted two simple tests for durability: repeated icing/deicing and relatively mild abrasion (see Materials and Methods). We compare our coatings' performance to other state-of-the-art icephobic coatings, such as commercial superhydrophobic surfaces (NeverWet), lubricant-infused surfaces (*8*), extremely low–surface-energy fluorodecyl polyhedral oligomeric silsesquioxane (POSS) coatings (*2*), and commercially available icephobic coatings (NuSil R-2180). As fabricated, our PU coating (coating CB; ρ^{CL} = 33 mol/m^3, 15 wt % safflower oil, θ_{adv}/θ_{rec} = 67°/29°, CAH = 38°) shows an order of magnitude reduction in τ_{ice} over the other state-of-the-art coatings considered here. Further, after just 10 icing/deicing cycles, all other coatings, except those fabricated here, exhibit ice adhesion strengths >200 kPa (with the exception of the commercial coating NuSil R-2180, which is a low ρ^{CL} PDMS). Additionally, after mild abrasion, only our PU coating remains icephobic, with an ice adhesion strength 2500% lower than any other coating relying on lubrication or low surface energy. We additionally tested our PDMS-based coating (coating OO), which can be repeatedly iced but is mechanically very poor, and a PU-based coating, where we intentionally added excess safflower oil (20 wt %) to form a lubricating, free-oil layer (coating CC; see Materials and Methods). There is statistically no difference in τ_{ice} values between the lubricated and interfacial slippage PU-based coatings initially or after 10 icing/deicing cycles (see Table 1, fig. S1C, and Fig. 5D). However, the lubricated PU coating easily delaminates from essentially all coated substrates (Fig. 5C, left inset) due to the presence of the free-oil layer. Similarly, slippery liquid-infused porous (SLIPS)–based surfaces using costly, fluorinated lubricants suffer a 10-fold increase in ice adhesion after just a few icing/deicing cycles (fig. S1A). Thus, there is a marked advantage to producing interfacial slippage–based icephobic coatings. Finally, note that a Si wafer treated with a PDMS-silane, a surface exhibiting interfacial slippage (*24*) due to pendent chains (*33*), also exhibits very low ice adhesion (τ_{ice} = 11 ± 4 kPa; see fig. S1D and Fig. 5D). In comparison, a Si wafer coated with a low surface energy fluorinated silane exhibits relatively high ice adhesion (τ_{ice} = 248 ± 57 kPa; fig. S1D). However, these thin silane coatings can be abraded away relatively easily (Fig. 5D).

To demonstrate the real-world potential of our durable icephobic surfaces, we conducted outdoor testing during the winter months of 2013 and 2014 in Ann Arbor, MI (see Materials and Methods). Over the 4 months of exposure, both snow and ice accreted severely on an uncoated glass panel. The coated panel often had snow settle on it, but all ice that formed was quickly sheared off even from mild winds (Fig. 5A) (*34*). After 4 months of exposure, the contact angles and τ_{ice}

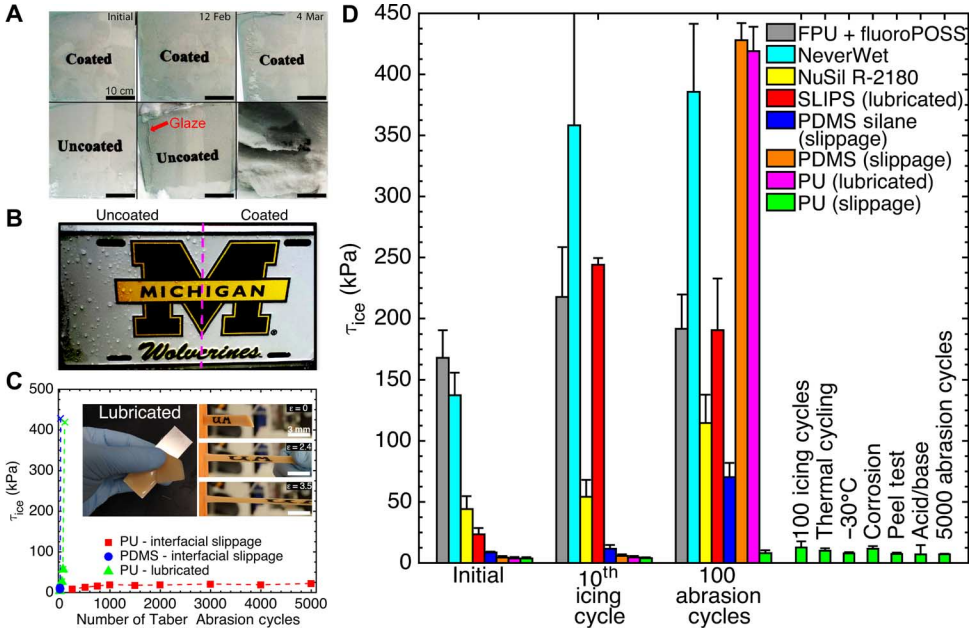

Fig. 5. Durability of the different icephobic coatings developed in this work. (**A**) Outdoor testing of a PDMS-based coating (coating NN; see Table 1) for 4 months during winter 2014. On 12 Febuary, the uncoated panel was covered with a ~7-mm layer of glaze, the type of ice with the strongest adhesion (*1*). No ice had accreted on the coated panel. On 4 March, snow followed a night of freezing rain, which completely covered the uncoated panel. The coated panel only had a small amount of accreted ice remaining. (**B**) Half-coated license plate during outdoor winter 2013 testing, with ice only accreted on the uncoated side. (**C**) Mechanical abrasion of three different icephobic coatings. The PDMS (coating NN) and lubricated PU (coating CC) were easily damaged and delaminated within 20 abrasion cycles, whereas the PU with interfacial slippage (coating CB) survives over 5000 cycles while maintaining low ice adhesion. (**D**) Comparison of coatings in this work with other state-of-the-art icephobic surfaces. Also, additional durability characterizations are presented for the PU coating with interfacial slippage. For details on each coating and test configuration, see Materials and Methods.

for the coated surface were the same as before testing, highlighting the coating's durability.

Finally, we conducted extensive durability testing (Fig. 5, C and D) on our icephobic polyurethane (coating CB) including Taber abrasion (ASTM D4060), acid/base exposure, accelerated corrosion (ASTM B117), thermal cycling, and peel testing (ASTM D3359) (see Materials and Methods). We also measured τ_{ice} over 100 icing/deicing cycles and evaluated the coating in a temperature range from −5° to −35°C (fig. S5B). After 5000 abrasion cycles, causing more than 600 μm of thickness loss, the coating remains icephobic because icephobicity is an inherent property of the coating. PDMS-based coatings (coating NN) or lubricated PU–based coatings (coating CC), though equally icephobic initially, are completely abraded away (and/or delaminated) after <20 cycles (Fig. 5C). The use of high surface energy elastomers, and the lack of a free-oil layer, allows us to create coatings that adhere very well to any underlying substrate. We observed no increase in τ_{ice} even after 10 successive peel tests on steel, copper, aluminum, and glass, or after thermal cycling between −10° and 70°C. The average ice adhesion strength for this coating after all durability testing is $\tau_{ice} = 9 \pm 2$ kPa. We additionally subjected our icephobic polyurethane to a tensile stress of 2.5 MPa, causing the elastomer to elongate by 350% without breaking or losing its icephobic properties (Fig. 5C, right inset, and movie S2). Additional tensile testing showed strains in excess of 1000% (fig. S3). The developed, extremely durable coatings can be spun, dipped, sprayed, or painted onto essentially any underlying substrate of any size. Finally, we had the extremely low ice adhesion strengths for multiple surfaces independently verified by Mode-I type (peel test) and Mode-II (zero-degree cone) adhesion testing at the U.S. Army's Cold Regions Research and Engineering Laboratory (CRREL) (see fig. S5A) (*35*).

Overall, in this work, we discuss two universal attributes, cross-link density and interfacial slippage, which can be used to systematically tailor ice adhesion for elastomeric surfaces, irrespective of material chemistry. It was found that interfacial slippage makes the biggest impact on the ice adhesion strength of low cross-link density elastomers. Using this understanding, we fabricate a range of different, mechanically durable, long-lasting icephobic surfaces from a wide range of material systems. We foresee such extremely durable, icephobic coatings having immediate, worldwide applications across various industrial sectors, academic disciplines, and engineering endeavors.

MATERIALS AND METHODS

Experimental design

The objective of this study was to understand the ice adhesion on elastomers, both with and without interfacial slippage. The materials were chosen to span a wide range of chemistries and mechanical properties. The evaluation of these materials involved characterizing their ice adhesion strengths, their mechanical properties, and their resultant durability. The ice adhesion measurements were designed such that an increase in ice adhesion due to repeated icing/deicing could be observed. The durability characterizations were designed such as to provide a wide range of potentially damaging exposures. By evaluating durability always with respect to ice adhesion, the potential for misrepresenting icephobic durability is avoided.

Synthesis

PDMS (Sylgard 184 or Sylgard 527, Dow Corning), silicone oil (5 to 10,000 cP; Sigma-Aldrich), and PMHS (Sigma-Aldrich) were used as received. Sylgard 184 is cross-linked in a 10:1 base/cross-linker ratio, and Sylgard 527 in a 1:1 ratio as per supplier instructions. The cross-linker for both of these products contains a copolymer of PDMS and PMHS, effectively controlling the cross-link density ρ^{CL}. Previous work has shown how mixing these two formulations can alter ρ^{CL} without deviating from stoichiometry (*36*). To increase ρ^{CL}, PMHS can be added along with a high temperature (150°C) cure. Curing at 80°C results in PMHS not effectively cross-linking within the PDMS elastomer, acting as a lubricant. To differentiate this effect, samples were either cured at 80°C for a minimum of 2 hours or at 150°C for 24 hours. To create PDMS filled with 25 wt % silicone oil while maintaining the same modulus as Sylgard 184, 10 wt % PMHS was required. To create a low ρ^{CL} PDMS with every chain chemically cross-linked, we used solvent extraction with toluene over a 2-week period to fully remove any uncross-linked chains. Excess toluene was changed out daily. Without such an arduous step, PDMS contains ~4% uncross-linked chains that act as lubricants (fig. S1 and Fig. 1) (*37*). To spin-coat these surfaces, solutions at a polymer concentration of 200 mg/ml were formed in hexane. Silicon wafers were rinsed with acetone and were then spin-coated with the different solutions at 1500 rpm for 60 s, followed by curing. For the dip-coated meshes, the substrates were submerged in the same solutions (200 mg/ml) for 45 min and blown dry to avoid pore clogging, followed by the same curing recipe as above.

PFPE (Sartomer CN4002) was cross-linked using 354-nm ultraviolet light under nitrogen with 1% 2-hydroxy-2-methylpropiophenone (Sigma-Aldrich) as the photoinitiator. SLIPS surfaces were recreated using published methods (*8*). FPU (Fluonova) was cross-linked using 8 wt % 1,6-hexamethylene diisocyanate as per the manufacturer's instructions. Krytox 100, 103, and 105 were purchased from DuPont and up to 25 wt % was added to the different polymers. The FPU was also cross-linked using an isocyanate-functionalized PDMS (Silmer NCO Di-100, Siltech) at a cross-linker ratio of 75/25 wt %. To this was added 100-cP silicone oil. Solutions were mixed in Vertrel XF or in chloroform at a concentration of 200 mg/ml. Vertrel XF is a non–ozone-depleting fluoro solvent that has replaced Asahiklin 225. Si wafers were rinsed with acetone, and the solutions were spin-cast at 1500 rpm for 60 s, followed by curing at 80°C overnight. The PU samples with known modulus (Smooth-On Inc.) were mixed at a 1:1 base/cross-linker ratio as per instructions. For lubricated samples, the oil (vegetable oil, Kroger; cod liver oil, Fisher; 100-cP silicone oil, Sigma-Aldrich; safflower oil, Jedwards International; or isocyanate-functionalized silicone oil, Silmer NCO Di-50) was added at levels of 1, 5, 10, 15, or 20 wt %. The rubber was cured at room temperature overnight. This rubber was altered using a 50/50 wt % ratio of the rubber cross-linker and an isocyanate-functionalized PDMS (Silmer NCO Di-100, Siltech) to improve silicone oil miscibility. The ρ^{CL} of the urethanes was altered by varying the type of isocyanate cross-linker or the urethane index, and/or through the addition of oil. Films were produced by either spin-coating or dip-coating glass slides in chloroform solutions at a solute concentration of 200 mg/ml, or spray-coating (500 mg/ml) or drop-casting without dilution. PS (M_w, 190,000; Scientific Polymer) was dissolved in toluene at a concentration of 200 mg/ml and to it was added silicone oil (AP 1000; Sigma-Aldrich), PMPS (Sigma-Aldrich), or low–molecular-weight PS (M_w, 200 or 540 g/mol; Scientific Polymer). PIB (M_w, 400,000 g/mol; Scientific Polymer) was dissolved in heptane at a concentration of 200 mg/ml and to it was added polybutene (M_n, ~920 g/mol; Sigma-Aldrich). Both PIB and PS samples

were spin-cast using the same recipe as above and then cured at room temperature for 24 hours. See Table 1 for a complete list of fabrication recipes and resulting surface properties.

To fabricate the surfaces for determining I^*, elastomers were made with and without oil, modifying one of the two surface, such that the cross-link densities matched to within 5% error. For example, the FPU with oil displayed a lower ρ^{CL} than the FPU without oil. Hence, we varied the ratio of different hexamethylene diisocyanate cross-linking agents until the desired modulus/cross-link density was achieved. Similar methods were used for PDMS (explained above) and PU samples.

For Fig. 3A, the lubricant surface was fabricated by spin-casting PMHS onto a Si wafer at 1500 rpm from a solution (200 mg/ml) in toluene. The lubricated surface is PDMS with a free layer of silicone oil (50 wt %, 100 cP) on the surface. The oil was added after curing to ensure that a thick, liquid layer remained present on the surface. For Fig. 3B, this same methodology was used with oils of varying viscosity, 5 to 10,000 cP for silicone oils in PDMS and 7 to 550 cP for Krytox oils in PFPE.

For Fig. 5D, the FPU was spin-cast with 20 wt % fluorodecyl POSS to create a smooth, low surface energy film. Whereas pure, spin-cast fluorodecyl POSS results in a relatively rough surface (due to crystallization), a 20 wt % film within the FPU is smooth and exhibits a surface energy of 11 mN/m, close to the surface energy of pure fluorodecyl POSS (*38*). The model superhydrophobic surface was the commercial product NeverWet (Rust-Oleum Inc.) and was sprayed on glass slides as per instructions. The two-part commercial icephobic coating R-2180 (NuSil Inc.) was dipped out of a hexane solution (1:1 ratio) at a concentration of 1000 mg/ml. The two silanized surfaces were Si wafers treated with either 1*H*,1*H*,2*H*,2*H*-heptadecafluorodecyltrichlorosilane (Gelest Inc.) or K13, a chlorine-terminated PDMS (M_w, 2000 to 4000; Gelest Inc.).

Photolithography

A 3-μm-thick layer of photoresist (SPR 220-3.0, Shipley) was spin-coated on a silicon wafer and baked for 90 s at 115°C. The lateral layouts of the micropattern were defined by 365-nm ultraviolet exposure (Karl Suss MA6 mask aligner) and developed in AZ 300 MIF. Inductively coupled plasma reactive-ion etching (STS Pegasus) formed ~30- and 75-μm-deep micropore arrays in the exposed regions, and the photoresist was stripped (Baker PRS 2000). To construct pillars of a precise thickness, two methods were adopted. For thick substrates, the uncured PDMS was poured onto the Si mold, degassed, and cured. For thin substrates, the uncured PDMS was spin-cast on the Si mold at 5000 rpm for 60 s with a ramp rate of 5 s. Glass slides were then placed atop the spin-cast layer. The PDMS was degassed to remove air bubbles between the glass slide and mold, and finally, the whole system was cured.

Ice testing

The ice adhesion strength τ_{ice} was measured using a custom setup described previously (*2*). Briefly, a force gauge was mounted to a movable stage. The gauge pushes the ice adhered to a substrate on top of a Peltier plate. The thickness of ice is ~5 to 8 mm, whereas the gauge contacts the surface <1 mm from the surface. Testing was done at −10°C except for a temperature study done between −5° and −35°C. Deionized water (0.5 ml) was used for all testing. Surfaces are allowed sufficient time to fully freeze before testing. For smooth coatings, τ_{ice} was found to be independent of the time between the water freezing completely and the ice being sheared off. τ_{ice} is the maximum force required to shear off a given area of ice. Force versus time curves were acquired for surfaces with τ_{ice} < 250 kPa by a Mark-10 force gauge, which has a minimum resolution of 0.0005 N. With this gauge, a τ_{ice} as low as 1.0 kPa can be measured with an accuracy of ±0.05 kPa. An Imada force gauge was used for surfaces with τ_{ice} > 250 kPa, which has a resolution of 0.1 N.

Outdoor testing and evaluation at the U.S. Army's CRREL

We coated the right half of a license plate with our icephobic PDMS (ρ^{CL} = 102 ± 5 mol/m^3, 25 wt % PMHS) and placed it outside during February 2013. Freezing rain occurred on the night of the 26th, and the plate was imaged the following morning. The uncoated side showed significant ice accretion, whereas all accreted ice on the coated side sheared off during the ice storm (Fig. 5B). Between December and March 2014, two glass panels (1 ft^2) were placed outdoors, one of them coated with our icephobic PDMS (ρ^{CL} = 76 ± 1 mol/m^3, 25 wt % silicone oil).

CRREL samples included a low ρ^{CL} PDMS coating (ρ^{CL} = 110 ± 5 mol/m^3), a low ρ^{CL} PDMS coating containing 25 wt % silicone oil (ρ^{CL} = 76 ± 1 mol/m^3), our polyurethane containing 15 wt % safflower oil (ρ^{CL} = 52 ± 1 mol/m^3), and our PDMS-modified polyurethane containing 10 wt % silicone oil (ρ^{CL} = 21 ± 1 mol/m^3). The CRREL ice adhesion setup involves aluminum tabs with an area of ice ~10 cm^2. Ice is grown from starter crystals under precisely controlled environmental conditions. A starter crack is formed at the base of the specimen and then the ice is pulled in a direction normal to the surface plane. In this way, Mode-I type fracture is evaluated.

Degree of cross-linking determination

Swelling studies were performed using toluene and acetone as the probe solvents. Substrates were submerged in excess toluene until a constant mass was achieved. Fully swollen substrates were patted dry before measurement to minimize any errors due to evaporation. Large-enough substrates were used so that the error associated with evaporated toluene vapor was <2%. Swollen samples were placed in an 80°C oven under vacuum to remove the toluene until the mass remained constant. In this manner, the extractable and permanent mass content could be discerned (*39*). Flory-Huggins interaction parameters for the FPU, PFPE, and PU were estimated by determination of their solubility parameter by swelling in a large number of solvents, as explained elsewhere (fig. S6) (*40*).

Mechanical characterization

To make dog-bone specimens, the uncured material (PDMS, FPU, or PU) was poured on fluoro-silanized glass panels 1 ft × 1 ft in area. For PDMS and PU, no solvent was added because the viscosity was low enough to produce smooth puddles of the liquid polymer. We added 1 ml of *n*-butyl acetate (Sigma-Aldrich) to the FPU per 5 g of FPU polyol and cross-linker. Once cured, dog-bone samples with dimensions outlined in ASTM D412, Die D were stamped out (*41*). Tensile testing was done on an MTS Insight 10 using a 10-kN load cell and a 56-mm gauge length. The crosshead was controlled at 10 mm/min. Mechanical abrasion was performed using a Linear Taber Abrasion machine with a CS-10 resilient abrader and a total weight of 1100 g. The abrader was refaced before each set of abrasion cycles using sand

paper (from Taber). Refacing was done at 25 cycles/min for 25 cycles. For abrasion, samples were clamped down and abraded for up to 5000 cycles at 60 cycles/min and a stroke length of 25.4 mm. For PDMS samples (Sylgard 184), the coating was completely removed after <50 cycles. Abrasion samples were drop-cast onto glass slides without dilution, giving a final coating thickness of ~2 mm.

Additional durability testing

Thermal cycling was performed by leaving a coated glass slide on a 70°C hotplate. After 24 hours, the ice adhesion at −10°C was measured, and this process was repeated 10 times. Probing the low temperature characteristics of the coatings was done by adjusting the Peltier plate from −5° down to −35°C.

Corrosion testing was done in accordance to ASTM B117 (*42*). Briefly, steel tabs measuring 25 mm × 75 mm were spray-coated at 500 mg/ml. The coated pieces are hung in a salt spray fog chamber (Bemco Inc.) kept at 35°C for 200 hours. A 25-mm scratch is made along the length of the coating so that the steel underneath is exposed. After the accelerated corrosion, the ice adhesion is measured.

A major concern for most hydrophobic polymers is their adhesion to substrates. We conducted standard peel tests in accordance with ASTM D3359 (*43*). A standard tape (Elcometer 99) is pressed on coated substrates using a rubber eraser. Substrates tested were steel, copper, aluminum, and glass. An elongated "X" pattern is cut into the coating before the tape is applied. After pulling the tape off quickly and at an angle of 180°, the coating is evaluated for removal from the substrate. On all substrates tested, our coating showed no sign of removal. We then repeated this process 10 times, followed by ice adhesion measurement.

Chemical stability was evaluated by submerging glass slides drop-cast with our icephobic polyurethane (with silicone, safflower, or vegetable oil) in 1.5 M HCl and NaOH solutions. The coated pieces were submerged for 5 min and then rinsed with copious amounts of deionized water. After drying, the ice adhesion was measured.

Microscopy/contact angle

Optical images were taken using a VistaVision VWR optical microscope with a 5× objective. Tapping mode AFM was conducted using a Veeco Innova instrument. Veeco TESPA tips and HiRes-C probes were used for imaging. Contact angles were measured using a Ramé-Hart 200-F1 goniometer. Measurements were made by advancing and receding a single droplet of liquid (~10 µl) from a 2-ml micrometer syringe (Gilmont). Averages from at least three independent measurements are reported.

Statistical analysis

Ice adhesion measurements were performed a minimum of 10 times successively on three different samples. Reported ice adhesion values are the average of these 30 measurements. Error bars on all plots are one SD. Cross-link density determination was performed on four separate samples and then averaged. The error in cross-link density is propagated through the Flory-Rehner analysis. The best fits for Fig. 1 are found through the method proposed by York *et al.* (*44*) to account for error in both dependent and independent variables. The ice adhesion measurements taken after durability characterization are the average of three successive measurements on three different samples. Contact angles are the average of three independent measurements on each sample.

SUPPLEMENTARY MATERIALS

Supplementary material for this article is available at http://advances.sciencemag.org/cgi/content/full/2/3/e1501496/DC1

Text

Fig. S1. Liquid layer surface degradation.

Fig. S2. Surface chemistry independence.

Fig. S3. Tensile test data.

Fig. S4. Interfacial slippage mechanism additional data.

Fig. S5. Icephobicity of coated meshes.

Fig. S6. Elastomer solubility parameter determination.

Movie S1. Ice releasing from its own weight.

Movie S2. Mechanical strength of icephobic PU.

REFERENCES AND NOTES

1. J. Shin, T. H. Bond, Surface roughness due to residual ice in the use of low power deicing systems, 31st Aerospace Sciences Meeting & Exhibit, Reno, NV, 11 to 14 January 1993.
2. A. J. Meuler, J. D. Smith, K. K. Varanasi, J. M. Mabry, G. H. McKinley, R. E. Cohen, Relationships between water wettability and ice adhesion. *ACS Appl. Mater. Interfaces* **2**, 3100–3110 (2010).
3. N. D. Mulherin, R. B. Haehnel, *Ice Engineering: Progress in Evaluating Surface Coatings for Icing Control at Corps Hydraulic structures* (U.S. Army Engineer Research and Development Center, Hanover, NH, 2003).
4. H. R. Baker, W. D. Bascom, C. R. Singleterry, The adhesion of ice to lubricated surfaces. *J. Colloid Sci.* **17**, 477–491 (1962).
5. S. Jung, M. Dorrestijn, D. Raps, A. Das, C. M. Megaridis, D. Poulikakos, Are superhydrophobic surfaces best for icephobicity? *Langmuir* **27**, 3059–3066 (2011).
6. K. K. Varanasi, T. Deng, J. D. Smith, M. Hsu, N. Bhate, Frost formation and ice adhesion on superhydrophobic surfaces. *Appl. Phys. Lett.* **97**, 234102 (2010).
7. S. B. Subramanyam, K. Rykaczewski, K. K. Varanasi, Ice adhesion on lubricant-impregnated textured surfaces. *Langmuir* **29**, 13414–13418 (2013).
8. P. Kim, T.-S. Wong, J. Alvarenga, M. J. Kreder, W. E. Adorno-Martinez, J. Aizenberg, Liquid-infused nanostructured surfaces with extreme anti-ice and anti-frost performance. *ACS Nano* **6**, 6569–6577 (2012).
9. H. Murase, K. Nanishi, On the relationship of thermodynamic and physical properties of polymers with ice adhesion. *Ann. Glaciol.* **6**, 146–149 (1985).
10. C. Wang, T. Fuller, W. Zhang, K. J. Wynne, Thickness dependence of ice removal stress for a polydimethylsiloxane nanocomposite: Sylgard 184. *Langmuir* **30**, 12819–12826 (2014).
11. L. Zhu, J. Xue, Y. Wang, Q. Chen, J. Ding, Q. Wang, Ice-phobic coatings based on silicon-oil-infused polydimethylsiloxane. *ACS Appl. Mater. Interfaces* **5**, 4053–4062 (2013).
12. K. Rykaczewski, S. Anand, S. B. Subramanyam, K. K. Varanasi, Mechanism of frost formation on lubricant-impregnated surfaces. *Langmuir* **29**, 5230–5238 (2013).
13. V. Hejazi, K. Sobolev, M. Nosonovsky, From superhydrophobicity to icephobicity: Forces and interaction analysis. *Sci. Rep.* **3**, 2194 (2013).
14. F. Arianpour, M. Farzaneh, S. A. Kulinich, Hydrophobic and ice-retarding properties of doped silicone rubber coatings. *Appl. Surf. Sci.* **265**, 546–552 (2013).
15. J. Chen, J. Liu, M. He, K. Li, D. Cui, Q. Zhang, X. Zeng, Y. Zhang, J. Wang, Y. Song, Superhydrophobic surfaces cannot reduce ice adhesion. *Appl. Phys. Lett.* **101**, 111603 (2012).
16. R. Dou, J. Chen, Y. Zhang, X. Wang, D. Cui, Y. Song, L. Jiang, J. Wang, Anti-icing coating with an aqueous lubricating layer. *ACS Appl. Mater. Interfaces* **6**, 6998–7003 (2014).
17. S. A. Kulinich, S. Farhadi, K. Nose, X. W. Du, Superhydrophobic surfaces: Are they really ice-repellent? *Langmuir* **27**, 25–29 (2011).
18. T.-S. Wong, S. H. Kang, S. K. Y. Tang, E. J. Smythe, B. D. Hatton, A. Grinthal, J. Aizenberg, Bioinspired self-repairing slippery surfaces with pressure-stable omniphobicity. *Nature* **477**, 443–447 (2011).
19. C. Urata, G. J. Dunderdale, M. W. England, A. Hozumi, Self-lubricating organogels (SLUGs) with exceptional syneresis-induced anti-sticking properties against viscous emulsions and ices. *J. Mater. Chem. A* **3**, 12626–12630 (2015).
20. Y. Wang, X. Yao, J. Chen, Z. He, J. Liu, Q. Li, J. Wang, L. Jiang, Organogel as durable anti-icing coatings. *Sci. China Mater.* **58**, 559–565 (2015).
21. M. K. Chaudhury, K. H. Kim, Shear-induced adhesive failure of a rigid slab in contact with a thin confined film. *Eur. Phys. J. E Soft Matter* **23**, 175–183 (2007).
22. K. Kendall, The adhesion and surface energy of elastic solids. *J. Phys. D Appl. Phys.* **4**, 1186 (1971).
23. A. Ghatak, L. Mahadevan, M. K. Chaudhury, Measuring the work of adhesion between a soft confined film and a flexible plate. *Langmuir* **21**, 1277–1281 (2005).
24. B.-m. Z. Newby, M. K. Chaudhury, H. R. Brown, Macroscopic evidence of the effect of interfacial slippage on adhesion. *Science* **269**, 1407–1409 (1995).
25. A. Ghatak, K. Vorvolakos, H. She, D. L. Malotky, M. Chaudhury, Interfacial rate processes in adhesion and friction. *J. Phys. Chem. B* **104**, 4018–4030 (2000).

26. K. B. Migler, H. Hervet, L. Leger, Slip transition of a polymer melt under shear stress. *Phys. Rev. Lett.* **70**, 287–290 (1993).
27. K. Vorvolakos, M. K. Chaudhury, The effects of molecular weight and temperature on the kinetic friction of silicone rubbers. *Langmuir* **19**, 6778–6787 (2003).
28. Y. B. Chernyak, A. I. Leonov, On the theory of the adhesive friction of elastomers. *Wear* **108**, 105–138 (1986).
29. P. J. Flory, J. Rehner Jr., Statistical theory of chain configuration and physical properties of high polymers. *Ann. N. Y. Acad. Sci.* **44**, 419–429 (1943).
30. N. Sombatsompop, Practical use of the Mooney-Rilvin equation for the determination of degree of crosslinking of swollen NR vulcanisates. *Sci. Asia* **24**, 199–204 (1998).
31. J. E. Mark, *Polymer Data Handbook* (Oxford Univ. Press, New York, ed. 2, 2009), pp. vii, 1250 pp.
32. J. Takadoum, *Materials and Surface Engineering in Tribology* (ISTE Ltd., London, 2008).
33. A. Galliano, S. Bistac, J. Schultz, Adhesion and friction of PDMS networks: Molecular weight effects. *J. Colloid Interface Sci.* **265**, 372–379 (2003).
34. J. Chen, R. Dou, D. Cui, Q. Zhang, Y. Zhang, F. Xu, X. Zhou, J. Wang, Y. Song, L. Jiang, Robust prototypical anti-icing coatings with a self-lubricating liquid water layer between ice and substrate. *ACS Appl. Mater. Interfaces* **5**, 4026–4030 (2013).
35. D. M. Cole, *ERDC-CRREL Nominal Mode I Ice Adhesion Testing* (Cold Regions Research and Engineering Laboratory, Hanover, NH, 2014).
36. R. N. Palchesko, L. Zhang, Y. Sun, A. W. Feinberg, Development of polydimethylsiloxane substrates with tunable elastic modulus to study cell mechanobiology in muscle and nerve. *PLOS One* **7**, e51499 (2012).
37. J. N. Lee, C. Park, G. M. Whitesides, Solvent compatibility of poly(dimethylsiloxane)-based microfluidic devices. *Anal. Chem.* **75**, 6544–6554 (2003).
38. A. Tuteja, W. Choi, M. Ma, J. M. Mabry, S. A. Mazzella, G. C. Rutledge, G. H. McKinley, R. E. Cohen, Designing superoleophobic surfaces. *Science* **318**, 1618–1622 (2007).
39. W. Chassé, M. Lang, J.-U. Sommer, K. Saalwächter, Cross-link density estimation of PDMS networks with precise consideration of networks defects. *Macromolecules* **45**, 899–912 (2012).
40. P. Schiopu, G. Ciobanu, G. Carja, G. Apostolescu, N. Apostolescu, C. Panait, G. Caruntu, A. Manea, The physicochemical properties of polyurethane membranes determined by swelling measurements. *Proc. SPIE* **7297**, 72970I–72974I (2009).
41. ASTM, in *ASTM D412-06a(2013), Standard Test Methods for Vulcanized Rubber and Thermoplastic Elastomers—Tension* (ASTM International, West Conshohocken, PA, 2013).
42. ASTM, in *ASTM B117, Standard Practice for Operating Salt Spray (Fog) Apparatus* (ASTM International, West Conshohocken, PA, 2011).
43. ASTM, in *ASTM D3359, Standard Test Methods for Measuring Adhesion by Tape Test* (ASTM International, West Conshohocken, PA, 2009).
44. D. York, N. M. Evensen, M. L. Martínez, J. De Basabe Delgado, Unified equations for the slope, intercept, and standard errors of the best straight line. *Am. J. Phys.* **72**, 367 (2004).

Acknowledgments

Funding: We thank K.-H. Kim and the Office of Naval Research for the financial support under grant N00014-12-1-0874. We also thank C. Y. Lee and the Air Force Office of Scientific Research for the financial support under grants FA9550-15-1-0329 and LRIR-12RZ03COR. We also thank the National Science Foundation and the Nanomanufacturing Program for supporting this work through grant #1351412. K.G. thanks the Department of Defense for a National Defense Science and Engineering Graduate Fellowship. **Author contributions:** K.G. designed and performed all experiments. S.P.R.K. performed AFM and photolithography. D.H.L. performed photolithography. E.T.D. performed abrasion and ice adhesion testing. J.M.M. provided the fluorodecyl POSS molecules and helped write the manuscript. K.G. and A.T. conceived the research, designed the experiments, and wrote the manuscript. **Competing interests:** The authors declare that they have no competing interests. **Data and materials availability:** All data needed to evaluate the conclusions in the paper are present in the paper and/or the Supplementary Materials. Additional data related to this paper may be requested from the authors.

Submitted 21 October 2015
Accepted 14 January 2016
Published 11 March 2016
10.1126/sciadv.1501496

Citation: K. Golovin, S. P. R. Kobaku, D. H. Lee, E. T. DiLoreto, J. M. Mabry, A. Tuteja, Designing durable icephobic surfaces. *Sci. Adv.* **2**, e1501496 (2016).

ScienceAdvances
AAAS

Designing durable icephobic surfaces

Kevin Golovin, Sai P. R. Kobaku, Duck Hyun Lee, Edward T. DiLoreto, Joseph M. Mabry and Anish Tuteja (March 11, 2016)

Sci Adv 2016, 2:.
doi: 10.1126/sciadv.1501496